T.2: X-ray diffraction studies of amorphous solids using ADXRD beamline (BL-12) on Indus-2 synchrotron source

A. K. Sinha and Pooja Gupta

Indus Synchrotrons Utilisation Division
E-mail: anil@rrcat.gov.in

1. Introduction:

Amorphous materials preserve short and intermediate range orders (of the order of a few atomic distances), unlike their crystalline counterparts, which show long range structural order. From configuration energy point of view, the amorphous material occupies one of many local minima unlike crystalline materials, which occupy a global minimum. Hence, when the amorphous system is subjected to some perturbation, like thermal annealing, charged particle/photon irradiation etc., they undergo from one local minimum to another changing the properties of the material, significantly. To understand and control the changes in the physical, magnetic, optical and electronic properties of the materials, due to the change in the amorphous structure, one has to understand and quantify the changes in 'amorphousness' of the material on perturbation. In literature, X-ray/neutron diffraction (XRD), Extended X-ray absorption Fine Structure (EXAFS) spectroscopy, Nuclear Magnetic Resonance (NMR) and Thermometric (DSC and DTA) techniques are used to study various aspects of amorphous systems.

XRD or neutron diffraction in an amorphous material results in a set of broad 'Halos' in contrast to a set of sharp Bragg peaks in the case of crystalline materials. The halos (in reciprocal or momentum space) are related to the pair distribution function (g(r)) in real space, which describes the spatial correlation between atoms in real space. These correlations give coordination number and distance of various pair of atoms. The coordination distances are related to strength of chemical bonding. In a polyatomic amorphous system, the concept of pair distribution function is extended such that the probability of finding one type of atom from another is called the partial pair distribution function. For example, for a diatomic amorphous system AB, the partial distribution functions A-A, B-B and A-B need to be obtained from diffraction data. These partial pair distribution functions give information on the chemical bonding between various atoms/ions. It is obviously not possible to obtain three partial pair distribution functions from one diffraction data. One way of overcoming this limitation is to use multi-wavelength anomalous diffraction (MAD) technique. It is well known that the atomic scattering factor, which decides the contribution of a particular atom to total diffraction cross section, varies significantly near the absorption edges of the atom, because of contribution due to the energy dependent anomalous correction to the normal atomic scattering cross section. The measurement, however, requires the tunability of the x-ray source because the XRD measurements have to be done at three different wave-lengths. Therefore, synchrotron is suitable for these measurements, because of its tunability. In short, the possibility of tuning the wavelength and also high energy photons are necessary for the determination of structure of amorphous systems.

Amorphous materials are important from the application as well as physics understanding points of view. Amorphous semiconductors are used in various applications like solar cells, IR detectors, optics, windows etc., and also in re-writable Cds/DVDs as well as non-volatile memory devices. Glasses are amorphous systems, which have wide variety of applications in windows, containers, lighting, optics etc. Soft magnetic amorphous alloys like FINEMET, HITPERM. NANOPERM etc. have applications in high frequency power transformers, SMPS, accelerator cavities, impedance tuners etc. In this article, we obtain the changes in pair distribution functions for a number of monatomic amorphous systems on various perturbations like thermal annealing, irradiation with electron etc., and correlated them to change in optical and magnetic properties. In the subsequent sections we present a theoretical background consisting of details of calculation of pair distribution function and radial distribution function, for a monatomic amorphous system. The method is extended to calculate partial pair distribution functions for a diatomic system. The subsequent section is on experimental details. The section gives brief description of the ADXRD beamline (BL-12), Indus-2 and the experimental station used for the measurement of XRD on amorphous systems. Results and discussion section, given next, gives the results of estimation of radial distribution function after various perturbations, on soft magnetic metallic glasses and polymers. The changes in the structure have been correlated with properties.

2. Theoretical Background:

2.1 The case of a mono-atomic amorphous sample:

The differential scattering cross section [1/N. (dσ(q)/dΩ)] per atom for monatomic system is related to the structure factor by the relation:

$$(1/N)[(d\sigma(q)/d\Omega)] = b^2_{coh} + b^2_{incoh} \qquad [1]$$

Where, b_{coh} and b_{incoh} are the coherent and incoherent parts of Rayleigh-Thomson scattering length (average), respectively. So b_{coh} is simply the average and b_{incoh} is the standard deviation of the scattering length distribution. Therefore, b_{incoh} should be 0 for monatomic sample and x-ray scattering.

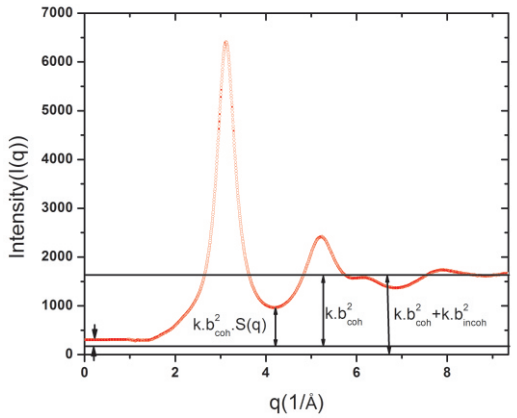

Fig. T.2.1: Measured XRD pattern of metallic glass after applying various corrections (background correction for the sample holder and absorption correction)

However, our system is not strictly monatomic. Also the data shows that b_{incoh} can't be neglected.

$$S(q) = \frac{1}{N} < \sum_{i,j=1} e^{qr_{ij}} >$$

is the static structure factor; where N is number of atoms contributing to scattering and q is the momentum transfer vector. Measured scattering intensity (after various corrections for fluctuation in photon beam intensity, scattering by the sample holder and absorption correction) is proportional to 1/N. ($d\sigma(q)/d\Omega$). We propose a method for the estimation of the constant of proportionality, from the corrected intensity versus q data. The analysis also gives b_{coh} and b_{incoh} and thus S(q) is obtained. Radial distribution function can then be obtained from the Fourier transformation of S(q) .

A measured x-ray scattering data for the as quenched soft magnetic alloy with composition $Fe_{72}Si_{4.8}B_{19.2}Nb_4$, after various corrections discussed above, is shown in Fig. T.2.1. We write (*k* is the constant of proportionality).

$$I(q) = k.(1/N).[d\sigma(q)/d\Omega] = k.b^2_{coh}.S(q) + k.b^2_{incoh} \qquad [2]$$

We have marked various components in Fig. 1. For large q (q tending to infinity); S (q) = 1. Therefore, From Eq. [2] and Fig. 1, we get

$k.b^2_{coh} + k.b^2_{incoh} = 1633$, where S(q) = 1 for large value of q, and

$k.b^2_{coh}.S(0) + k.b^2_{incoh} = 300$

S(0) can be estimated using a thermodynamic limit: $S(0) = \rho.\chi.k_B.T$; where ρ is the atomic number density, χ is the isothermal compressibility and k_B is the Boltzman constant. Since majority component of our sample is Fe. We have used cast iron data for estimation of S(0). We get $S(0) = 5 \times 10^{-2}$ and $k.b^2_{incoh}$ and $k.b^2_{incoh}$ are estimated to be 230 and 1403 respectively. We now calculate S(q) using Eq. (2) andthe same is plotted in Fig. T.2.2. Function D (r) defined as:

$$D(r) = \int_0^\infty q.(s(q)-1).\sin(qr).dq \qquad [3]$$

Slope of D(r) for low r gives the average number density (ρ_0); required in the calculation of Radial Distribution Function (RDF = $4\pi r^2\rho_0$ g(r)), where the function g(r) given by

$$g(r) - 1 = (1/2\pi r^2\rho_0)\int_0^\infty q.(s(q)-1).\sin(qr).dq \qquad [4]$$

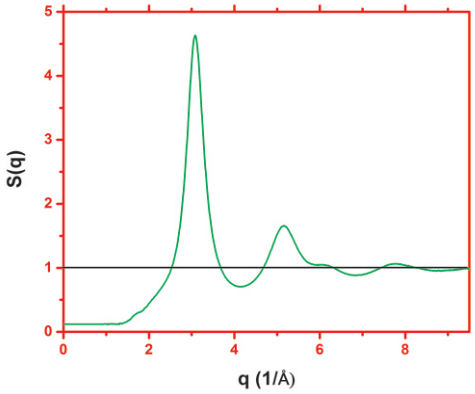

Fig. T.2.2: Static structure factor as a function of q = (4π/λ) sinθ

In Fig. T.2.3, we plot radial distribution function, alongwith $4\pi r^2\rho_0$ as a function of r. This shows that atoms are distributed in space in coordination shells. n_i, the number of atoms in a co-ordination shell can be obtained by integrating RDF(r) between two consecutive minima.

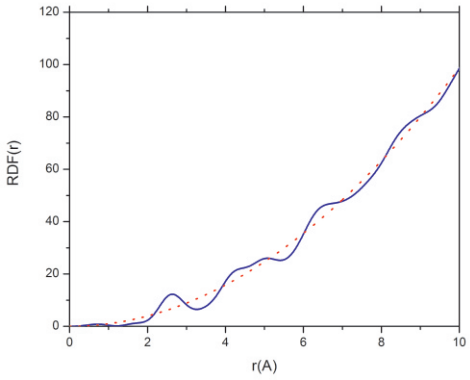

Fig. T.2.3: RDF = $4\pi r^2\rho_0.g(r)$ for the sample whose XRD is shown in Fig.T.2.1. g(r) is the pair distribution function.

Therefore; $$n_1 = \int_{r1}^{r2} RDF(r).dr$$

Where, r1 and r2 defines the first co-ordination shell.

2.2 The case of a diatomic amorphous system:

We extend equation [1] above for a diatomic amorphous system and relate total Interference Function (F(q, E)) to partial structure factor S(q) by the matrix equation:

$$F = A\,(S-1)$$

Where, F is a 3x1 column matrix consisting of elements F_1, F_2 and F_3. These are interference functions measured at three photon energies (E_1, E_2 and E_3), two of which are in anomalous energies. A is a 3x3 matrix whose elements are a_{ij} (i, j = 1,2,3). The matrix elements a_{ij} are given as below:

$$a_{11} = C_x^2.\, b_{x1}^2,\ a_{21} = C_y^2.\, b_{y1}^2,\ a_{31} = C_x.C_Y(b_{x1}\, b_{Y1}^* + b_{x1}^*\, b_{Y1})$$

$$a_{12} = C_x^2.\, b_{x2}^2,\ a_{22} = C_y^2.\, b_{y2}^2,\ a_{32} = C_x.C_Y(b_{x2}\, b_{Y2}^* + b_{x2}^*\, b_{Y2})$$

$$a_{13} = C_x^2.\, b_{x3}^2,\ a_{32} = C_y^2.\, b_{y3}^2,\ a_{33} = C_x.C_Y(b_{x3}\, b_{Y3}^* + b_{x3}^*\, b_{Y3})$$

Here, C_X and C_y are the fractional atomic concentrations of the constituent elements in diatomic material (XY), such that $C_X + C_Y = 1$. b_{X1} and b_{X2} are given by the equations:

$$b_{X1}(q,E_1) = r_e\,\{Z_X.\, f_0^X(q) + f'(E_1) + i.\, f''(E_1)\}$$

$$b_{X2}(q,E_2) = r_e\,\{Z_X.\, f_0^X(q) + f'(E_2) + i.\, f''(E_2)\}$$

$$b_{X3}(q,E_3) = r_e\,\{Z_X.\, f_0^X(q) + f'(E_3) + i.\, f''(E_3)\}$$

Here, f' and f'' are the real and imaginary parts of the energy dependent atomic scattering factors, respectively. f_0 is the normal atomic scattering factor which varies as 1/q from 1 (at q = 0) to 0 (at q = infinity). f'' is obtained from simple normalization of measured absorption data and f' is calculated from the K-K transformation of f''. Z is the atomic number of element X. Matrix elements b_{Y1}, b_{Y2} and b_{Y3} are also calculated using equations similar to those given above. However, the anomalous corrections are valid only for the element, whose absorption energies have been probed (in this case it is element x). For the other element Y, f' and f'' are zero. Hence, $b_{Y1} = b_{Y2} = b_{Y3} = r_e Z_Y.\, f_o^Y(q)$.

S is the 3×1 column matrix, whose elements are S_{XX}, S_{YY} and S_{XY}; where, these are partial structure factors. Finally, Interference functions F(q,E) are related to measured and normalized scattering cross section by the relation

$$F(q,E) = (1/N).[\,(d\sigma\,(q,E)/d\Omega) - (C_x^2.\, b_x^2 + C_Y^2.\, b_x^2 + C_x.C_Y\,(b_x b_Y^* + b_x^* b_Y)]$$

3. Experimental:

X-ray diffraction measurements on amorphous materials were carried out in Angle Dispersive X-ray diffraction beamline (BL-12) at Indus-2 synchrotron radiation source. The beamline operates between 5 and 22 keV photon energy range with a typical energy resolution (E/ΔE) of 8000 (at ~8keV photon energy). The beamline delivers about 1E9 to 1E10 photons per second at the experimental station and the size of the photon beam is 0.5mm x 0.5mm. The beamline consists of a Si(111) based double crystal monochromator (DCM) and pre and post adoptive mirrors for collimation/focusing on meridional direction. The focusing in the sagittal direction is achieved by bendable second crystal of the DCM. The XRD measurements reported in this article have been performed in transmission mode, using an Image Plate area detector (Mar 345 Dtb). The data is then reduced to conventional I(2θ) form using software Fit2D. The beam energy was calibrated periodically by the Cu and Zr k-edges of pure Cu and Zr foils.

4. Results and Discussion:

4.1. Correlation between magnetic and structural properties of Cu-free alloys on annealing:

In this example, we present the evolution of the amorphous structure of Cu free FINEMET alloy with composition $Fe_{72}B_{19.2}Si_{4.8}Nb_4$, on isochronal annealing for one hour at various temperatures between 200 and 600 °C. In literature it has been reported that the nano crystalline Cu precipitates in FINEMET alloys on annealing is mainly responsible for the change in magnetic properties. However the evolution of amorphous matrix also should have some contribution to the change in magnetic properties. In normal FINEMET alloys this effect gets overshadowed by the presence of large changes in magnetic properties due to nano size Cu precipitates. Therefore, we have taken Cu free FINEMET alloy to study the change in magnetic properties due to evolution of amorphous matrix alone. Measured SXRD data of the as quenched sample (sample No. #1) and the samples annealed at 200°C(#2), 400°C(#3) and 600°C(#4) are shown in Fig. T.2.4. Although the sample is a multiatomic system, the contribution to total atomic cross section by Si and B are negligibly small, because these are low Z elements. Nb also may not contribute significantly because of its small atomic concentration. Therefore, we have treated the system as a monatomic system. As discussed in section 2, RDF (r), for all the samples were calculated (from their SXRD patterns) and are presented in Fig. T.2.5.

We find that the number of atoms in the first shell does not change on annealing. Also the position at which the maxima of the distribution occur remains unchanged on annealing. The width of the first shell remains more or less constant (0.71± 0.01) for samples #1 to #3.However, for the sample annealed at 600°C (sample #4), the width decreases to 0.59 ± 0.01. This shows that the first shell remains unaltered for annealing up to 400°C. The decrease in width indicates that the sample #4 is tending towards crystalline state. This is in agreement with the x-ray diffraction data, shown in Fig. T.2.4.

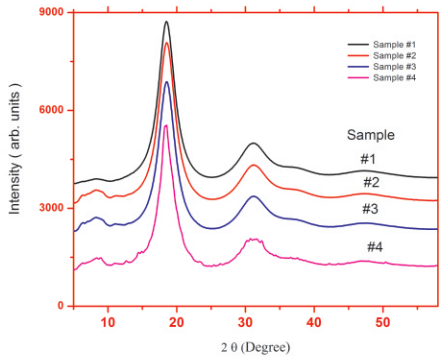

Fig. T.2.4: XRD pattern of samples #1 to #4.

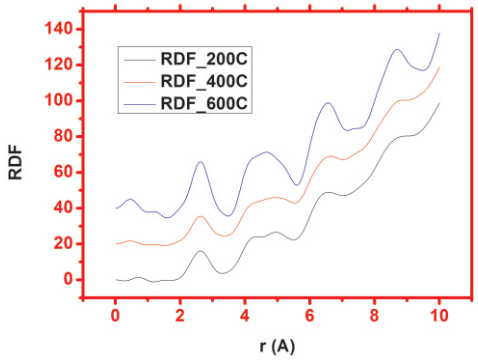

Fig. T.2.5: RDF of samples #2, #3 and #4 annealed at 200 C, 400 C and 600 C, respectively.

The data clearly shows crystalline peaks riding over the amorphous background. The parameters (width, position of maxima and area) of the first coordination shell remains more or less unchanged for samples #1 to #3, whereas, the magnetic properties were found to change significantly. Therefore, some structural properties must have altered, if the change in magnetic properties has some structural origin. In order to verify that we have studied the second coordination shell. Here, we find that the number of atoms increases slightly and the position of the maxima decreases with increasing annealing temperature. The width of the second shell initially remains constant (1.70±0.01) for sample #1 to #3 and then decreases to 1.53 for sample #4. The changes in the widths are similar for both first and second shells. Magnetic properties of the metallic glass like remenance field, saturation magnetisation and hysteresis loss were found to correlate with the structural parameters of the second co-ordination shell.

4.2 Electron irradiation induced changes in structural properties of Fe and Co based metallic glasses:

Metallic glass ribbons of nominal compositions $Co_{72}Si_{4.8}B_{19.2}Nb_4$ (Labelled as sample A) and $Fe_{72}Si_{4.8}B_{19.2}Nb_4$ (Labelled as sample B) were prepared by quenching and a part of the ribbons were subjected to electron irradiation (700keV, 1.5mA), using DC accelerator. The RDF of the as quenched and electron irradiated samples (A and B) are shown in Figs.T.2.6(a) and T.2.6(b), respectively. We see increase in amplitude of the RDF function for both the samples, on electron irradiation.

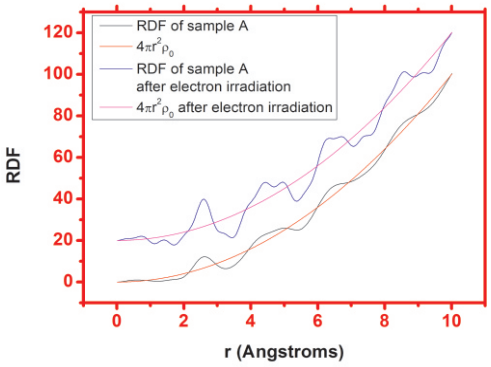

Fig. T.2.6(a): RDF for sample #A (Co72Si4.8B19.2Nb4) before and after electron irradiation.

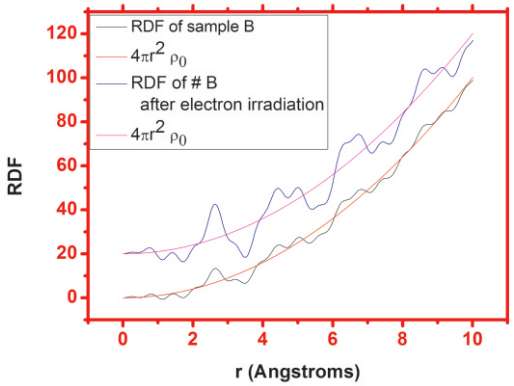

Fig. T.2.6(b): RDF for sample #B($Fe_{72}Si_{4.8}B_{19.2}Nb_4$) before and after electron irradiation.

We find that the average number of atoms in the first co-ordination shell increases slightly (about 10%) in both the cases. The width of the first co-ordination shell decreases drastically from 1.1 angstrom to ~0.55 angstrom, after

electron irradiation. This is an indication of a more ordered phase on electron irradiation. The saturation magnetisation is found to increase significantly, on electron irradiation.

4.3 Structural modification of polymethyl methacrylate (PMMA) due to electron irradiation:

PMMA is one of the highest resolution positive organic resist for electron beam lithography (EBL) as well as for deep UV, X-ray and focused ion beam micro-lithography processes. The limiting factor for the resolution for EBL results from the interaction of the electrons with the resist molecules. Electron irradiation in PMMA results in changes in the amorphousstructure and subsequently other properties like optical, thermal, electrical etc. The PMMA film exhibits amorphous nature having broad diffraction maxima, as shown in Fig.T.2.7 for unirradiated PMMA sample as well as for samples irradiated with 1mC/cm2 (irradiated 1) and 2mC/cm2 (irradiated 2).To quantify the changes in structure, we have performed RDF analysis. RDF for the three samples are shown in Fig.T.2.8.

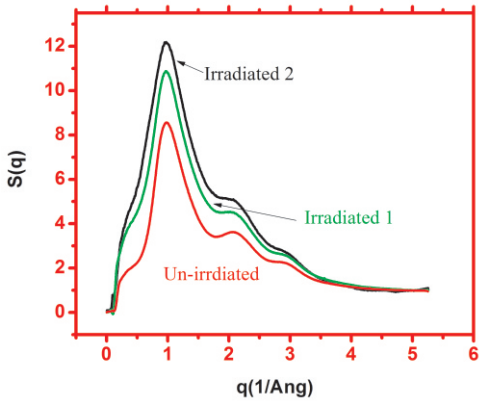

Fig. T.2.7: Structure factor calculated from the measured XRD data after various corrections and normalization.

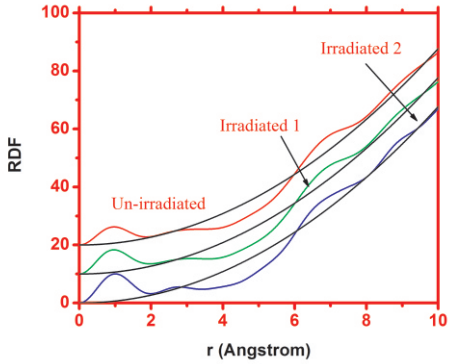

Fig. T.2.8: RDF for un-irradiated and electron irradiated samples with dose 1 mC/cm^2 (irradiation 1) and 2 mC/cm^2 (irradiation 2).

The co-ordination number and the first co-ordination distance for the un-irradiated as well as the irradiated sample with lower dose (1mC/cm2) are about the same. This indicates that lower dose does not change the amorphous structure. Whereas, the sample with higher dose of electron, shows slight increase (~10%) in the first co-ordination distance and corresponding decrease in the co-ordination number, compared to the un-irradiated sample.

4.4 Cu clustering in the amorphous phase of Fe-Cu-Nb-Si-B alloy:

Fe-Cu-Nb-Si-B alloys follow a very interesting nanocrystallisation process upon suitable heat treatment. In the early stage of annealing, below the crystallization temperature (up to ~ 450 C), small amounts of Cu and Nb strongly affect the nucleation as well as growth process and results in theformation of nanocrystalline structure. As Cu is non-soluble in Fe, it precipitates out from the amorphous phase and form rich aggregates/ clusters. Presence of Nb in alloy reduces the Cu solubility in alloy and thus accelerates the Cu precipitation upon heat treatment, refines Cu clusters. For annealing in the temperature range of 500-600 C, the number density of these Cu clusters decreases while a second fraction has been formed as a crystalline bcc Fe-(Si) phase. At 650 Cand higher temperatures, Fe-B phases are formed.

Various studies are reported in literature to understand how Cu acts to refine the scale of crystallized microstructures in these alloys. It was suggested that these Cu clusters act as heterogeneous nucleation sites by providing a template of regularly spaced atoms upon which the Fe and Si atoms crystallize. Since Cu atoms substitute for Fe atoms and their clustering does not affect distribution of other solutes, this cluster formation causes a concentration fluctuation of Fe. Because of this concentration fluctuation, the density for the nuclei of the bcc crystalline phase increases significantly. Direct evidence for this mechanism is very difficult to obtain because the sizes of the Cu clusters and bcc Fe-Si grains are both extremely fine.Although the earlier atom probe analysis, and EXAFSinvestigations credibly showed the presence of fcc-Cu clusters prior to the onset of the crystallization reaction in the Fe-Si-B-Nb-Cu amorphous alloy, how Cu clusters stimulate nucleation of the bcc Fe-Si has been a mere speculation.Attempts have also been made to clarify the spatial distribution, size and onset temperature of Cu enriched clusters by SANS and DSC measurements. It has been found that there is an optimum Cu concentration for grain refinement, beyond which the grain size again increases. Attempts have been made to understand this optimum Cu concentration in terms of the difference between clustering temperature and the crystallization temperature. It was suggested that large difference between Cu clustering

temperature and the crystallization temperature will result in coarsening of Cu clusters and thus reducing their number. Thus the Cu clusters, which precipitate in the amorphous state of these alloys, play an important role to device the final microstructure. Most of the studies reported in the literature explain Cu clustering in the partially/fully crystallized state of Fe-Cu-Nb-Si-B alloy. Ohnuma et al. have studied Cu clustering for the specimen annealed at 400 Cfor 60 min, but there are no reports on the detailed structural evolution of the amorphous state of such an alloy. In order to understand the role of Cu in controlling the size of nanocrystals and to devise optimum composition, it is necessary to understand the kinetics of Cu clustering in the pure amorphous state of these materials.

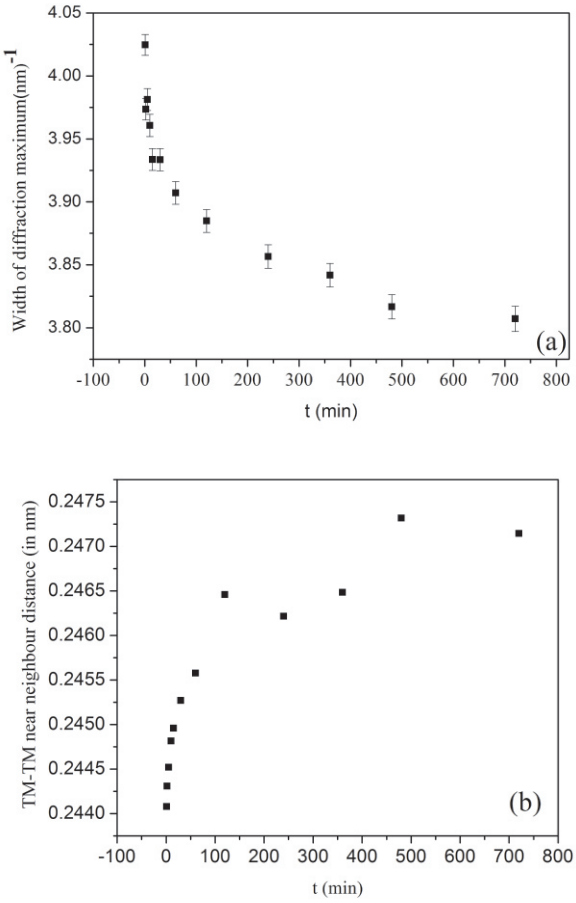

Fig. T.2.9: (a) Width of the diffraction maximum as a function of annealing time (b) Average TM-TM near neighbour distance as a function of annealing time.

Present study was undertaken with an effort to understand the kinetics of Cu clustering in the pure amorphous state of Fe-Cu-Nb-Si-B alloy. Structural evolution of Fe-Cu-Nb-Si-B alloy in its amorphous state was studied in detail by isothermal annealing well below the crystallization temperature using WAXS measurements. WAXS measurements confirm that no crystallization takes place even after the highest annealing time of 720 min. The as-quenched sample presents a broad hump, which is characteristic of the amorphous phase and can be fitted with a Lorentzian function. Detailed fitting and analysis of all the profiles show that the full width at half maximum, which is a measure of the disorder in the system, decreases with increasing annealing time (Fig. T.2. 9a).

This may be connected to a structural relaxation in the amorphous phase, which results in an increased topological order in the system. The position of the first broad maximum can be used to get distance between the near neighbour atoms (x_m) in the amorphous phase. Since the x-ray scattering from the metalloid atoms is significantly weak as compared to that from the transition-metal (TM) atoms, x_m as obtained in the present case should be the average TM–TM near-neighbor distance. This value increases unexpectedly, as shown in Fig. T.2.9b, while structural relaxation is expected to result in the annihilation of defects and excess free volume and thus should result in a decrease in the TM-TM near neighbour distance. Therefore the observed increase in x_m cannot be understood in terms of structural relaxation. In the amorphous state the structural relaxation should result in relieving of internal stresses and increase in the compositional homogeneity and then the result obtained in the present study may be understood in terms of clustering of Cu atoms: in case Cu precipitates out of the amorphous matrix the transition metal concentration of the amorphous phase would decrease, resulting in an increase in the average TM-TM near neighbour distance, as observed here.

4.5 Radial distribution function of theCu-free HITPERM $Fe_{40.5}Co_{40.5}Nb_7B_{12}$ alloy in its pure amorphous state:

Fig. T.2.10 shows the representative radial distribution function (RDF) for the sample annealed at 658 K, where the alloy remains in the pure amorphous phase.In general, the position of the first broad maximum can be used to calculate the distance between the nearest neighbor atoms (Xm) in the amorphous phase using the relation,

where c is a constant and generally taken as 1.23. Upon comparison of the transition metal-transition metal (TM-TM) distance as obtained from the RDF, the value of c was found to be ~1.31 for the present set of experiments. This has been used

to estimate the TM-TM distance, from the amorphous contribution, in the partially crystalline samples.

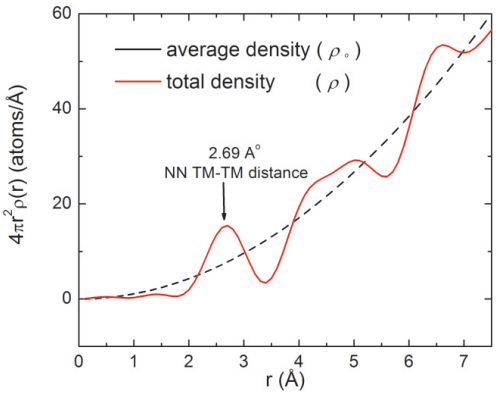

Fig. T.2.10: Radial distribution function of the $Fe_{40.5}Co_{40.5}Nb_7B_{12}$ alloy in its pure amorphous state.

4.6 Micro-structural evolution of the $Fe_{81-x}Co_xNb_7B_{12}$ alloy as a function of increased Co composition:

XRD measurements were performed on all the as-quenched alloy compositions using the photon beam energy of 20.2 keV and by keeping sample-to-image-plate distance as 85.6 mm. The image plate data files were integrated using FIT2D, incorporating polarization correction. Fig. T.2.11 shows XRD pattern of the as-spun $Fe_{60.75}Co_{20.25}Nb_7B_{12}$ (F3C1), $Fe_{54}Co_{27}Nb_7B_{12}$ (F2C1), $Fe_{40.5}Co_{40.5}Nb_7B_{12}$ (F1C1), $Fe_{27}Co_{54}Nb_7B_{12}$ (F1C2), $Fe_{20.25}Co_{60.75}Nb_7B_{12}$ (F1C3) alloys, demonstrating micro-structural evolution of the alloy as a function of increased Co composition.

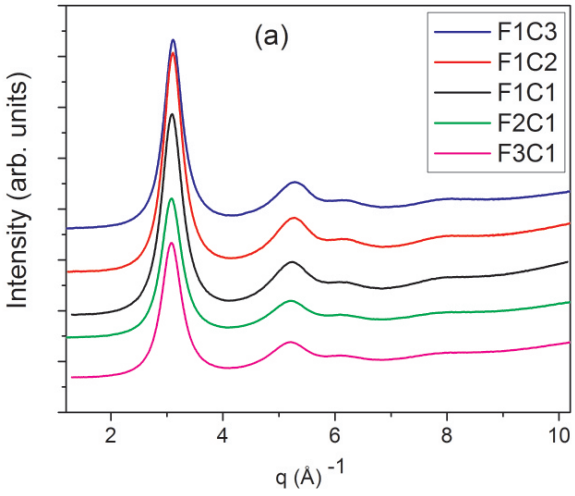

Fig. T.2.11: XRD pattern of as spun $Fe_{81-x}CoxNb_7B_{12}$ alloy as a function of increased Co composition.

All the XRD spectra show four distinct broad halos, signifying amorphous structure in the as-quenched state. The first broad halo for all the compositions (Fig.T.2.11) can be well fitted with a Lorentzian function. Detailed fitting and analysis of all the profiles show that the full width at half maximum (FWHM), which is a measure of the disorder in the system, shows an increase with increasing Co concentration up to ~ 40.5 % in the FeCoNbB alloy, beyond this value it decreases. Thus Co addition 40.5% facilitate topological ordering in the system (Fig. T.2.12).

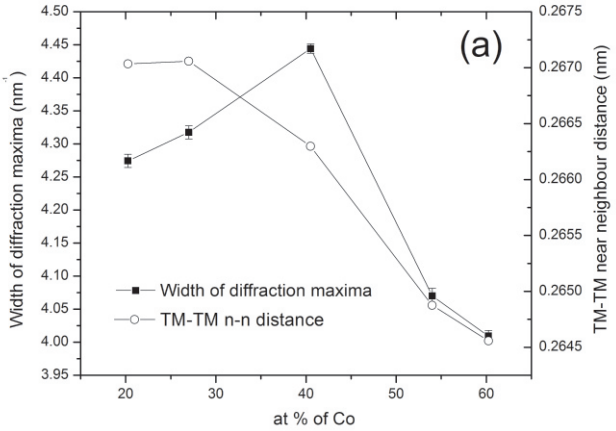

Fig. T.2.12 Width of the diffraction maximum and average TM-TM near neighbour distance as a function of Co content.

The position of the first broad maximum can be used to calculate the distance between the nearest neighbor atoms (X_m) in the amorphous phase using the relation given in previous section. Since the X-ray scattering from the metalloid atoms is significantly weak as compared to that from the transition-metal atoms, X_m, as obtained in the present case should be the average TM-TM near-neighbor distance.

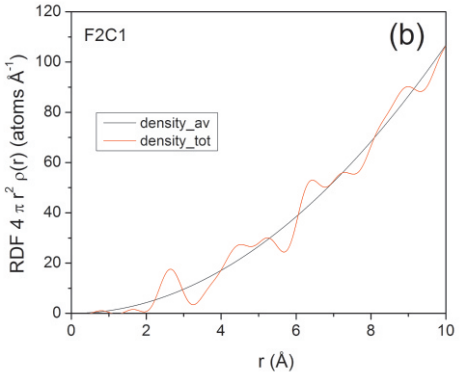

Fig. T.2.13: Representative radial distribution function for F2C1 alloy.

As shown in Fig. T.2.12, the TM-TM nearest neighbour distance decreases with increase in the Co concentration. This decrease in atomic volume (i.e. Xm) possibly suggests the tendency of ordering with increasing Co concentration in the alloy. Thus Co addition may result in relieving of internal stress and increase in the compositional homogeneity.

The radial distribution function (RDF) has been calculated for all the alloy compositions in the amorphous state and one of the representative graphs (for F2C1 alloy) is shown in Fig. T.2.13. Ratio of second to first near-neighbor atomic distances is ~1.7, which is comparable with the previously known amorphous foils.

Conclusions:

In this article, a detailed method for Fourier transformation of XRD data have been discussed, in a pedagogic manner, for monatomic amorphous system. This gives the pair distribution function (Radial distribution function), which describes the correlation between a pair of atoms in amorphous systems. The co-ordination number and distance are obtained from an arbitrarily chosen central atom. The coordination distance may be related to the strength of chemical bond between the pair of atoms. We have applied the methodology to a number of amorphous system like soft magnetic alloys, polymers etc., to study the changes in their amorphous structure on various perturbations such as thermal annealing and electron irradiation. The changes in structure have been correlated with the changes in their properties. The method have been extended to study the amorphous structure of a binary alloys, by using anomalous x-ray diffraction.

Acknowledgements:

Authors acknowledge Dr. P. D. Gupta and Dr. P. A. Naik for their support and encouragement. Acknowledgements are also due to Dr. T. Ganguli, Miss Pragya Tiwari and Dr. S. N. Kane for their association in different parts of the reported work. Dr.ArchnaSagdeo, Shri Anuj Upadhyay and Shri M. N. Singh are acknowledged for their help during XRD measurements.

References:

1. Sinha A. K., Singh M. N., Upadhyay Anuj, Satalkar M., Shah M., Ghodke N., Kane S. N. and Varga L. K., *AppliedPhysicsA* 118, 291 (2015).
2. Kane S. N., Satalkar M., Ghosh A., Shah M.,Ghodke N., Pramod R., Singh A. K., Singh M. N.,Dwivedi J., Coisson M.,Celegato F.,Vinai F.,Tiberto P.,Varga L. K., *Journal of Alloys and Compounds* 615, S324 (2014).
3. Gupta Pooja, Ganguli Tapas, Švec P., Sinha A.K., Gupta A., ŠvecSr P.,Singh M.N., Reddy V.R. and Deb S.K., *Journal of Applied Physics* 114, 083516 (2013).
4. Gupta Pooja, Ganguli Tapas, Gupta A., Sinha A. K., Deb S. K., Svec Jr. P. and Franco V., *Journal of Applied Physics 111,113518 (2012).*
5. Gupta Pooja,Gupta A., Shukla A.,Ganguli Tapas, Sinha A. K., Principi G. and Maddalena A., *Journal of Applied Physics 110, 033537(2011).*
6. Tiwari P., Srivastava A. K.,Khattak B. Q., Verma S.,Upadhyay A., Sinha A .K.,Ganguli T., Lodha G.S. and Deb S.K., *Measurement 51,1 (2014).*
7. Sinha A.K., Jaiswal A., Gupta P., Upadhyay A., Kumar A., Singh M.N., Gupta R.K., Kane S.R., Verma A., Deb S. K., *J. Phys.: Conf. Series425,072017 (2013).*
8. StachurskiZ.H., *Materials 4, 1564 (2011).*
9. Fischer H.E.,Barnes A.C., Salmon P.S.,*Rep.Prog.Phys. 69, 233 (2006).*